INTERNATIONAL JOURNAL FOR NUMERICAL METHODS IN FLUIDS
Int. J. Numer. Meth. Fluids 2002; **40**:231–240 (DOI: 10.1002/fld.273)

An optimal control approach to optical flow computation

A. Borzì[1,*,†], K. Ito[2] and K. Kunisch[1]

[1]*Institut für Mathematik, Karl-Franzens-Universität Graz, Heinrichstr. 36, 8010 Graz, Austria*
[2]*Department of Mathematics, North Carolina State University, Raleigh, NC 27695-8205, U.S.A.*

SUMMARY

An optimal control approach for determining optical flow is presented. The new framework differs from preceding approaches in that it does not require differentiation of the data. A numerical algorithm that solves the optimality system consisting of hyperbolic and elliptic partial differential equations is presented. Copyright © 2002 John Wiley & Sons, Ltd.

KEY WORDS: optical flow; optimal control

1. INTRODUCTION

An optical flow is the field of apparent velocities in a sequence of images. From this flow, information about the spatial arrangement of objects and the rate of change of this arrangement ought to be obtained. One assumes that objects represented in the image are flat surfaces, that they are uniformly illuminated, and that reflectance varies smoothly and has no spatial discontinuities [1]. Under these assumptions, the image brightness of an object point remains constant in the images when the object moves. That is, the total time derivative of the brightness at each point (x, y) at time t is zero:

$$\frac{\partial I}{\partial t} + u\frac{\partial I}{\partial x} + v\frac{\partial I}{\partial y} = 0 \tag{1}$$

where $I = I(x, y, t)$ denotes the image brightness at (x, y) and t, and $\mathbf{w} = (u, v)$ represents the optical flow vector. Equation (1) is referred to as the *optical flow constraint* (OFC). For a derivation of the model we refer to References [1, 2].

Given a sampled sequence of image frames $\{Y_k\}_{k=1}^N$, at times t_k, most techniques for optical flow calculations first approximate the spatio-temporal derivatives, (I_x, I_y, I_t), and aim at solving (1) for $\mathbf{w}$. Equation (1) can only be solved uniquely with the addition of an auxiliary

*Correspondence to: A. Borzì, Institut für Mathematik, Karl-Franzens-Universität Graz, Heinrichstr. 36, 8010 Graz, Austria.
†E-mail: alfio.borzi@uni-graz.at

Contract/grant sponsor: Supported in part by the SFB 03 'Optimization and Control'

Received May 2001
Revised November 2001

constraint or regularization term. The novelty of our formulation is given by the fact that the image frames Y_k and the corresponding variable I in mathematical model (1) for the optical flow are separate quantities. Consequently, the optimal control formulation does not require differentiation of the data and we distinguish between the sampling rate of the images and the time discretizing of I in the numerical realization of our algorithm.

To solve the optimal control problem, we derive the associated first-order optimality conditions. These result in a system of two forward–backward hyperbolic equations and two elliptic equations together with appropriate initial and boundary conditions. We solve the optimality system by combining a second-order explicit TVD scheme and a second-order multigrid method in a segregated loop algorithm. Results of numerical experiments with synthetic and real image sequences demonstrate the ability of the optimal control formulation to determine optical flow from two or more image frames.

2. OPTIMAL CONTROL FRAMEWORK FOR OPTICAL FLOW

In this section we formulate an optimal control problem for optical flow. Consider a sequence of image frames $\{Y_k\}_{k=1}^N$ sampled at increasing time steps, $t_k = (k-1)\,\mathrm{D}T$, $k = 1, 2, \ldots, N$, where $t_1 = 0$ and $t_N = T$. Here, a uniform sampling rate is assumed and set equal to one, $\mathrm{D}T = 1$. Each frame is assumed to be defined on a rectangle which defines the spatial domain Ω. The space–time box in which the optical flow takes place is $\Omega \times [0, T]$. We define the following *constrained minimization problem*: Find $\mathbf{w}$ and I such that

$$\begin{aligned} I_t + \mathbf{w} \cdot \nabla I = 0 \quad &\text{in } Q = \Omega \times (0, T] \\ I(\cdot, 0) = Y_1 \end{aligned} \tag{2}$$

and minimize the cost functional

$$J(I, \mathbf{w}) = \frac{1}{2} \int_\Omega \sum_{k=1}^{N} |I(x, y, t_k) - Y_k|^2 \, \mathrm{d}\omega + \frac{\alpha}{2} \int_Q \left| \frac{\partial \mathbf{w}}{\partial t} \right|^2 \mathrm{d}q + \frac{\beta}{2} \int_Q (|\nabla u|^2 + |\nabla v|^2) \, \mathrm{d}q + \frac{\gamma}{2} \int_Q |\nabla \cdot \mathbf{w}|^2 \, \mathrm{d}q$$

Here, α, β, and γ are predefined non-negative weights. The first term in J is the least-squares term requiring that $\mathbf{w}$ is chosen such that $I(\cdot, t_k, \mathbf{w})$ approximates Y_k at the sampling times. The second and third terms are regularization terms which are necessitated by the fact that the determination of a temporally and spatially varying vector field $\mathbf{w}$ from the data is under determined. These regularization terms are analogously used in References [1, 3]. They are motivated by the assumption that $\mathbf{w}$ is smooth with respect to t and the spatial variables x and y. We introduce the last term in order to enforce the filling-in property [2]. That is, consider the case that all velocities on the border of a small subregion are the same. The points in the interior of the subregion should be assigned the same value too. A way of expressing this property is to penalize by $\int_Q |\nabla \cdot \mathbf{w}|^2 \, \mathrm{d}q$.

We use the method of Lagrange multipliers [4] to turn the constrained minimization problem defined above into an unconstrained one and we focus on the necessary optimality conditions of first order. This results in the optimality system:

$$I_t + \mathbf{w} \cdot \nabla I = 0 \quad \text{with } I(\cdot, 0) = Y_1 \tag{3}$$

$$p_t + \nabla \cdot (\mathbf{w}p) = \sum_{k=2}^{N-1} [\delta(t - t_k)(I(\cdot, t_k) - Y_k)] \quad \text{with } p(\cdot, T) = -(I(\cdot, T) - Y_N) \tag{4}$$

$$\alpha \frac{\partial^2 u}{\partial t^2} + \beta \Delta u + \gamma \frac{\partial}{\partial x}(\nabla \cdot \mathbf{w}) = p \frac{\partial I}{\partial x} \tag{5}$$

$$\alpha \frac{\partial^2 v}{\partial t^2} + \beta \Delta v + \gamma \frac{\partial}{\partial y}(\nabla \cdot \mathbf{w}) = p \frac{\partial I}{\partial y} \tag{6}$$

where δ denotes the Dirac δ-function. The interpretation of (4) is

$$p_t + \nabla \cdot (\mathbf{w}p) = 0 \quad \text{on } t \in (t_{k-1}, t_k) \quad \text{for } k = 2, \ldots, N \tag{7}$$

$$p(\cdot, t_k^+) - p(\cdot, t_k^-) = I(\cdot, t_k) - Y_k \quad \text{for } k = 2, \ldots, N - 1 \tag{8}$$

Note that while the optical flow constraint equation is marching forward in time, the adjoint optical flow equation is marching backward. The last two elliptic equations are referred to as the optimality condition.

Concerning boundary conditions for $\mathbf{w}$, we consider cases where no objects are traversing the boundaries of the image frame, thus we restrict the admissible optical flow fields to satisfy homogeneous Dirichlet boundary conditions on the spatial boundary and natural boundary conditions at the temporal boundaries of Q, i.e.

$$\mathbf{w} = 0 \text{ on } \partial\Omega, \text{ for } t \in [0, T], \quad \frac{\partial \mathbf{w}}{\partial t} = 0 \text{ for } t = 0 \text{ and } t = T, \text{ in } \Omega \tag{9}$$

In case the image does not satisfy homogeneous Dirichlet boundary conditions, it can be enlarged by assigning the value zero within a strip along the boundary. Other choices of boundary conditions are possible; see, e.g. Reference [2]. Our choice of the boundary conditions at $t = 0$ and at $t = T$ is the same as in Reference [3].

3. THE METHOD OF HORN & SCHUNCK

The method of Horn and Schunck [1] aims at computing optical flow velocity from spatio-temporal derivatives of image brightness. Though this scheme was one of the first methods for determining optical flow, it is still competitive and is one of the most used methods both in its original form or with various modifications; see References [1–3, 5]. This method combines optical flow constraint (1) with a global smoothness term defining a *unconstrained minimization problem*; minimizing

$$\int_Q [(I_t + \mathbf{w} \cdot \nabla I)^2 + \lambda^2(|\nabla u|^2 + |\nabla v|^2)] \, \mathrm{d}q \tag{10}$$

In the original formulation [1] all quantities in (10) are considered to be defined at an intermediate time step ($\mathrm{D}T/2$) between two sampled images from which the spatio-temporal

derivatives (I_x, I_y, I_t), where I equals Y, are obtained by numerical differentiation. A minimum of (10) necessarily satisfies the Euler equations:

$$\lambda^2 \Delta u - I_x(I_t + uI_x + vI_y) = 0 \tag{11}$$

$$\lambda^2 \Delta v - I_y(I_t + uI_x + vI_y) = 0 \tag{12}$$

where Δ is the Laplace operator and homogeneous Dirichlet boundary conditions (9) are used. The choice of the regularization parameter λ specifies the degree of smoothness of the solution. We shall take $\lambda = 0.5$ as suggested in Reference [2] for good results.

To solve Euler equations (11) and (12), one usually discretizes Δ by a nine-point star discrete Laplace operator and (I_t, I_x, I_y) are replaced by centred finite differences; see References [1–3]. The resulting discrete Euler equations are solved by a block-Gauss–Seidel iteration.

In using (11) and (12), an accurate computation of the spatio-temporal derivatives is necessary to obtain reliable results. Accuracy is not sufficient; in fact in Reference [5], examples are given where the use of accurate discretization schemes for differentiation provide wrong results unless the velocity of the pattern (i.e. $\mathbf{w}$) is close to the ratio of the spatial to the temporal sampling, that is, $u \approx \mathrm{D}X/\mathrm{D}T$ and $v \approx \mathrm{D}Y/\mathrm{D}T$. This may be related to the fact that in order to solve numerically optical flow equation (1), the following CFL-like condition must be satisfied:

$$\tau \leqslant \frac{C_{\mathrm{CFL}}}{\max(|u|_{\max}/h, |v|_{\max}/h)} \tag{13}$$

Here τ is the time step size, h the spatial mesh size, and $0 < C_{\mathrm{CFL}} \leqslant 1$ is the CFL number.

The discussion above outlines a limitation of the Horn & Schunck scheme which is not present in our approach, since the time discretization for the numerical realization of (3)–(6) and the sampling times for the images are independent.

4. NUMERICAL ALGORITHM

The numerical solution of the optimality system presents difficulties due to the presence of two coupled subsystems with different characters. Experience from computational fluid dynamics has shown that an efficient solution process can be obtained by using two different types of solvers for the two subsystems, each designed to solve one of the two blocks accurately and efficiently. Efficient and accurate methods to solve the optical flow constraint equation and the adjoint equation are given by explicit high-order TVD schemes [6]. An efficient and accurate solution of the elliptic control system is obtained by using the FAS multigrid method [7]. The coupling between the hyperbolic and the elliptic subsystems is obtained by repeated application of a *segregation loop* as follows:

Segregation loop for solving the optimal control problem (3)–(6).

1. Apply the Horn & Schunck method for a starting approximation to $\mathbf{w}$.
2. Solve the optical flow constraint equation to obtain I.
3. Solve (backward) the adjoint optical flow constraint equation to obtain p.
4. Update the right-hand sides of the elliptic system.

5. Apply a few V-cycles of multigrid to solve the control equations.
6. Go to 2 and repeat I_{loop} times.

We next discuss steps 2–5 of the segregation loop in some detail. Consider a space–time grid denoted by $Q_{h,\tau} = \Omega_h \otimes \Theta_\tau$. We follow the standard procedure and normalize the distance between pixels to one. Thus the spatial discretization is linked to the availability of pixel information by setting the space mesh size $h = \mathrm{D}X = \mathrm{D}Y = 1$. The grid spacing in the time direction is denoted by τ and is defined as a fraction of $\mathrm{D}T = 1$. A mesh point in $Q_{h,\tau}$ is represented by three indices (i, j, κ), $i, j = 1, 2, \ldots, L$, and $\kappa = 1, 2, \ldots, K$.

We implement an explicit second-order upwind TVD scheme with the 'Superbee' limiter of Roe for step 2; see Reference [6] for the details. We have chosen Superbee based on our numerical experience. We use fixed time steps for an easy (grid) coupling with the other equations of the optimality system. The CFL bound is taken equal to $C_{\text{CFL}} = 0.5$. The adjoint equation is solved by the same method as described for step 2 by reversing time. To numerically realize the delta impulses in the sense of (8) we use a splitting technique at t_k, i.e. we have

$$p(\cdot, t_\kappa) = p(\cdot, t_\kappa^+) - (I(\cdot, t_k) - Y_k) \quad \text{for } t_{\kappa+1} = t_k, \ \ k = 2, \ldots, N-1$$

to compute $p(\cdot, t_\kappa)$. Here $p(\cdot, t_\kappa^+)$ is obtained by solving (7) (backwards) for one time step with initial condition $p(\cdot, t_{\kappa+1})$.

In the segregation loop, we solve for I and store its value at each time step. Then, we solve for the adjoint variable p and set up and store $p\nabla I$ at each time step, that is, the source term of the control equations. To calculate the derivatives with respect to space of the image function, we use a centred five-point formula. Tests with three-point formulae gave similar results.

The system of the two elliptic equations arising in the optimal control framework is discretized by finite difference methods. Consider the elliptic equation for u^h:

$$\begin{aligned} &\alpha \frac{u^h_{i,j,\kappa+1} - 2u^h_{i,j,\kappa} + u^h_{i,j,\kappa-1}}{\tau^2} + \beta\{\Delta^h u^h\}_{i,j,\kappa} + \gamma \frac{u^h_{i+1,j,\kappa} - 2u^h_{i,j,\kappa} + u^h_{i-1,j,\kappa}}{h^2} \\ &= \left[p \frac{\partial I}{\partial x}\right]_{i,j,\kappa} - \gamma \frac{v^h_{i+1,j+1,\kappa} - v^h_{i+1,j-1,\kappa} - v^h_{i-1,j+1,\kappa} + v^h_{i-1,j-1,\kappa}}{4h^2} \end{aligned} \tag{14}$$

where $i, j = 2, \ldots, L-1$, and $\kappa = 2, \ldots, K-1$. Here we continue to use h for easier reading of the formulae, although $h = 1$. Further $\tau = T/K$ is chosen such that CFL condition (13) is satisfied. We discretize the second term of (14) by the usual five-point difference Laplacian. The last term of Equation (14) represents a second-order accurate discretization of $\gamma \partial^2 v / \partial x \partial y$. In a similar fashion we obtain the discretization of the elliptic equation for the v^h component of the optical flow. The boundary conditions are given by $u^h_\kappa = v^h_\kappa = 0$ on $\partial\Omega_h$, $\kappa = 1, 2, \ldots, K$. The Neumann boundary conditions at $t = 0$ and $t = T$ for u^h and v^h are discretized by first-order differences.

In order to solve efficiently the space–time elliptic system for (u, v) we implement the *full approximation scheme* (FAS) multigrid method of Brandt [7]. This method results in a solution process with optimal computational and storage complexity. In the case of Equation (14) (and the one corresponding to the v variable) a strong anisotropy in the coefficients of the

problem is present when $\tau \ll h$. For this reason t-line relaxation based on the Thomas algorithm [6] is used as smoother in the multigrid process. The Neumann boundary conditions are then enforced to update the variable values at the Neumann boundaries. For the multigrid coarse grid correction process, in order to transfer the residuals on coarser grids, a half-weighted restriction is used, whereas the solution on coarser grids is transferred using the simple injection. For the prolongation, we use the trilinear interpolation operator.

Convergence of the iterative procedure forming the segregation loop (Steps 2–6) is an independent issue which is investigated elsewhere.

5. NUMERICAL EXPERIMENTS

In the optical flow community, an angular measure of error is used to measure optical flow accuracy. One considers the pattern displacement as a space–time direction vector $\mathbf{w} = (u, v, 1)$ in units of (pixel,pixel,frame). The corresponding three-dimensional direction vector is denoted by $\hat{w} = \mathbf{w}/|\mathbf{w}|$. The *space–time orientation error* between the correct velocity $\mathbf{w}^{\mathrm{c}}$ and an estimate $\mathbf{w}^{\mathrm{e}}$ is given by $\psi^E = \arccos(\hat{w}^{\mathrm{c}} \cdot \hat{w}^{\mathrm{e}})$ [1]. We denote by $\psi^E_{i,j,\kappa} = \arccos(\hat{w}^{\mathrm{c}}_{i,j,\kappa} \cdot \hat{w}^{\mathrm{e}}_{i,j,\kappa})$ the error function ψ^E evaluated at grid point (i, j, κ). This measure of the optical flow error is made global by considering the *mean orientation error*

$$\tilde{\psi} = \frac{1}{KL^2} \sum_{\kappa=1}^{K} \sum_{i,j=1}^{L} \psi^E_{i,j,\kappa}$$

at the space–time mesh points of the evolving images. On this set of points, we also compute the maximum modulus of the functions u and v denoted by $|u|_{\max}$ and $|v|_{\max}$, respectively, to establish the accuracy of the optical flow with respect to the maximal velocity. In the tables we also report the tracking error, denoted by $\|I - Y\|^2$, and defined by

$$\sum_{\kappa=1}^{K} \sum_{i,j=1}^{L} (I^{t_k}_{i,j} - Y(x_i, y_j, t_k))^2 \tag{15}$$

Finally, in order to validate the divergence term in the cost functional, we also report the value of the discrete version of the divergence term.

Note that because we work in terms of pixels, the value of the tracking errors and costs may appear to be excessively large. Normalized values are obtained by dividing the reported values by their respective volumes.

5.1. Experiments with sequences of synthetic images

A standard test for optical flow solvers with synthetic images is given by a square moving with velocity $(u_{\mathrm{c}}, v_{\mathrm{c}})$. At time t, the frames are defined by means of the following function:

$$I(x, y, t) = \begin{cases} 1 & x^{\mathrm{l}}_t \leqslant x \leqslant x^{\mathrm{r}}_t \text{ and } y^{\mathrm{l}}_t \leqslant y \leqslant y^{\mathrm{u}}_t \\ 0 & \text{otherwise} \end{cases} \tag{16}$$

where x^{l}_t and x^{r}_t are the x-co-ordinates of the left and right vertical edges of the square, respectively, and y^{l}_t and y^{u}_t are the y-co-ordinates of the lower and upper horizontal edges of the square, respectively.

Table I. Moving square: $(u_c, v_c) = (1.5, 2)$. Dependence on α and γ.

Dependence on α; $\beta = 0.25$, *and* $\gamma = 0.1$				
α	$\|u\|_{\max}, \|v\|_{\max}$	$\bar{\psi}$	$\|I - Y\|^2$	$\|\mathrm{div}(w)\|^2$
1	2.78, 3.10	13.58	333.1	13.5
5	1.70, 2.15	14.21	68.0	3.8
10	1.71, 2.12	15.31	90.4	4.1
Dependence on γ; $\alpha = 5.0$, *and* $\beta = 0.25$				
γ	$\|u\|_{\max}, \|v\|_{\max}$	$\bar{\psi}$	$\|I - Y\|^2$	$\|\mathrm{div}(w)\|^2$
0	1.74, 2.19	14.81	65.5	0
0.25	**1.67**, **2.10**	**13.5**	**71.9**	**3.2**
0.5	1.64, 2.04	12.54	78.4	2.6
1	1.61, 1.99	11.21	91.0	2.1
H & S	2.49, 2.51	19.09		

We consider a translating square on a sequence of five frames of 64×64 ($L = 64$) pixels and $N = 5$ and $T = 4$ with $K = 64$ time sub-intervals of size $\tau = T/64$. That is, every $l_t = 16$ steps, a new image frame is given. In the multigrid solver five levels are used. The coarsest grid is a $4 \times 4 \times 4$ space–time grid, refined by halving the mesh size.

We take $(u_c, v_c) = (1.5, 2)$ and the images of the square are given by (16) with $x_t^l = x_0 + u_c t$, $x_t^r = x_0 + u_c t + 20$, $y_t^l = y_0 + v_c t$, and $y_t^u = y_0 + v_c t + 20$, where $(x_0, y_0) = (20, 20)$. Notice that the modulus of the optical flow velocity is such that the CFL condition (i.e. (13) with τ replaced by $\mathrm{D}T = 1$ and $h = \mathrm{D}X = \mathrm{D}Y = 1$) is not satisfied by the given image sequence. However, (13) is satisfied with τ utilized for the optimal control scheme.

Results of our experiments are reported in Table I where one can observe that the solution obtained with our method differs considerably from that obtained with the Horn & Schunck scheme. In fact, the optimal control solution is a good approximation to the two different velocity components while the components of the Horn & Schunck solution are too large and almost equal to each other. Compare the values in bold fonts with the last line in Table I. We show the ability of our approach to determine the optical flow also in the case where only two image frames are given. This case is encountered in the field of image registration; see Reference [8]. We use the same discretization setting as in the previous case, with $N = 2$, $T = 1$, and $\tau = \frac{1}{64}$. Control applies through the final observation, Y_N, and the tracking error measures the error on the final observation, $\|I(\cdot, T) - Y_N\|^2$. The translating square as defined above is used. Results for this case are reported in Table II. Here, because of the absence of tracking information for intermediate time steps, a bigger role is played by the second-order time derivative term of the control functions in the cost functional. A larger value of α results in a reduction of the tracking error at the cost of larger errors in the optical flow estimate: An over-regularization effect occurs. For this reason, best results are obtained if the value of α is kept smaller than in the multiple frames cases and larger values of β and γ are chosen. To conclude this section let us observe that in all experiments the optimal control

Table II. Two sample images: $(u_c, v_c) = (1.5, 2)$. Dependence on α and γ.

Dependence on α; $\beta = 0.25$, *and* $\gamma = 0.1$				
α	$\|u\|_{\max}, \|v\|_{\max}$	$\bar{\psi}$	$\|I - Y\|^2$	$\|\mathrm{div}(w)\|^2$
0.5	1.79, 2.33	23.02	11.2	6.0(−1)
1	1.97, 2.55	24.07	10.4	1.3
5	2.32, 2.55	26.43	25.9	3.1
Dependence on γ; $\alpha = 1.0$, *and* $\beta = 0.25$				
γ	$\|u\|_{\max}, \|v\|_{\max}$	$\bar{\psi}$	$\|I - Y\|^2$	$\|\mathrm{div}(w)\|^2$
0	2.06, 2.58	24.61	9.5	0
0.5	1.74, 2.34	22.55	12.8	7.6(−1)
1	**1.59**, **2.11**	**21.33**	**14.8**	**5.0(−1)**
2	1.48, 1.85	19.83	18.9	3.2(−1)
H & S	2.46, 2.47	27.10		

algorithm attains a substantial reduction of the tracking error within ten loops. With $I_{\text{loop}} = 10$, in all cases, a reduction of at least three orders of magnitude of the discrete L_2 norms of the residuals of all equations of the optimality system occurs. Further steps of the segregation loop results in a smaller improvement of the tracking error and of the estimate of the optical flow.

5.2. *Experiments with sequences of real images: the taxi sequence*

A known benchmark for verification of optical flow solvers is the 'Hamburg Taxi Sequence'; see Reference [2]. It consists of a sequence of frames of a taxi coming from the right in the main road and turning right into a side street in Hamburg (Germany). One photo of the sequence and the corresponding brightness pattern are depicted in Figure 1. We consider a sequence of (the first) five photos of the moving taxi taken at regular intervals ($T = 4$). The space–time computational domain is a $128 \times 96 \times 128$ grid, where 128 time subdivisions are taken in the time direction. This grid can be obtained from a coarse $4 \times 3 \times 4$ mesh by halving the mesh size 6 times. Our algorithm is applied with $\alpha = 5.0$, $\beta = 0.25$, $\gamma = 0.25$, and $I_{\text{loop}} = 10$. In Figure 1 the optical flow computed with the optimal control approach at $t = 2$ is presented. Comparing with the solution obtained with the Horn & Schunck method, our approach provides a smoother and more uniform optical flow for the taxi sequence. Moreover, the incompressibility term $\int_Q |\nabla \cdot \mathbf{w}|^2 \, \mathrm{d}q$ leads to improved filling-in features.

6. CONCLUSIONS

We presented a new approach to optical flow computation that is based on an optimal control framework. Specific features of the method are that it does not require differentiation of the data and that the sampling time of the image frames and the time discretization of the optical flow equation are separate. We solved the optimality system by means of a segregation

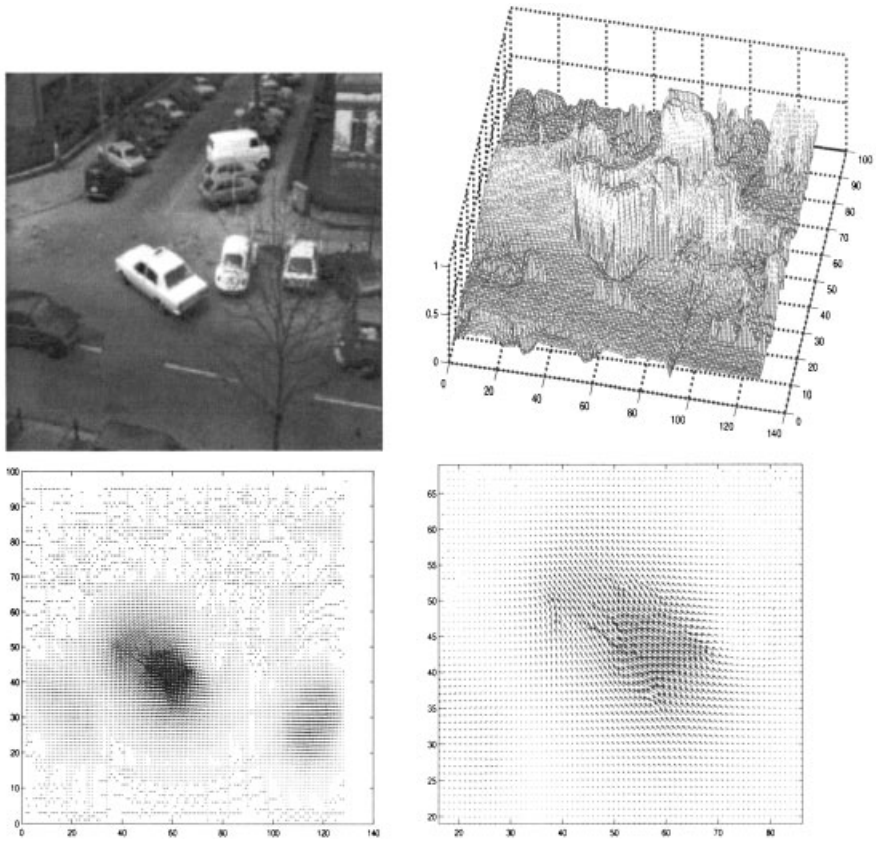

Figure 1. First frame of the taxi sequence (top left); the corresponding brightness distribution (top right). Optical flow for the taxi sequence (bottom left). Close-ups of the solution containing the region of the taxi (bottom right).

loop algorithm involving an explicit second-order TVD upwind scheme and the FAS multigrid method.

REFERENCES

1. Horn BKP, Schunck BG. Determining optical flow. *Artificial Intelligence* 1981; **17**:185–204.
2. Barron JL, Fleet DJ, Beauchemin SS. Performance of optical flow techniques. *International Journal of Computer Vision* 1994; **12**:43–77.
3. Weickert J, Schnörr C. Optical flow calculations with nonlinear smoothness terms extended into the temporal domain. *University of Mannheim*, *Computer Science Series*, *Technical Report*, vol. 4, 1999.
4. Lions JL. *Optimal Control of Systems Governed by Partial Differential Equations*. Springer: Berlin, 1971.
5. Battiti R, Amaldi E, Koch C. Computing optical flow across multiple scales: an adaptive coarse-to-fine strategy. *International Journal of Computer Vision* 1991; **6**:133–145.
6. Hirsch C. *Numerical Computation of Internal and External Flows*, vols. 1 and 2. Wiley: Chichester, 1990.
7. Brandt A. Multi-level adaptive solutions to boundary-value problems. *Mathematics of Computation* 1977; **31**: 333–390.

8. Rueckert D, Hayes C, Studholme C, Summers P, Leach M, Hawkes DJ. Nonrigid registration of breast MR images using mutual information. In *Medical Image Computing and Computer-Assisted Intervention—MICCAI'98*, Wells WM, Colchester A, Delp S (eds), *Lecture Notes in Computer Science*, vol. 1496. Springer: New York, 1998; 1144–1152.

